A

Fig. 4. (A) The optical amplitude A times the cosine of the optical phase $\cos\phi$ for a single tracked pulse as measured through the heart of the waveguide for the entire scan range (Fig. 2D). a.u., arbitrary units. A clear fringe pattern with an envelope is observed. The envelope is slightly asymmetric owing to the different chirps of the signal and reference pulses. **(B)** False color representation of $A\cos\phi$ as a function of the lateral position in the plane of the sample. The area depicted is an enlargement of a small part of the actual scan; the location is indicated by the double arrow in (A). It is clear that the wavefronts in the image are straight, indicating plane wave propagation. The periodicity of the wavefronts yields the wavelength inside the structure associated with the central optical frequency of the spectrum of the femtosecond laser pulse. The wavelength is found to be 415 ± 6 nm, corresponding to a phase velocity of $1.97 \pm 0.03 \times 10^8$ m/s.

probe is kept at a fixed location while the interference is measured as a function of the position of the optical delay line. In this way, it is even possible to measure the transmission function of a certain stretch of photonic structure by carrying out this procedure on either end of the stretch and comparing the results.

tive index method. The material dispersion is taken into account as $n^2(\lambda) = A^2 + B\,\lambda^2/(\lambda^2 - C^2)$, with $A = 0$, $B = 3.8693$, and $C = 119.61$ nm for Si_3N_4 (TM polarization) and $A = 1$, $B = 1.0998$, and $C =$ 92.431 nm for SiO_2. The calculations use the locally measured width and height of the ridge.

References and Notes

1. J.-C. Diels, W. Rudolph, *Ultrashort Laser Pulse Phenomena: Fundamentals, Techniques, and Applications on a Femtosecond Time Scale* (Academic Press, San Diego, CA, 1996).
2. *Photonic Crystals and Light Localization in the 21st Century*, C. M. Soukoulis, Ed. (NATO Science Series, Kluwer Academic, Dordrecht, Netherlands, 2001).
3. S. John, N. Aközbek, *Phys. Rev. Lett.* **71**, 1168 (1993).
4. A. M. Steinberg, P. G. Kwiat, R. Y. Chiao, *Phys. Rev. Lett.* **71**, 708 (1993).
5. C. Spielmann, R. Szipöcs, A. Stingl, F. Krausz, *Phys. Rev. Lett.* **73**, 2308 (1994).
6. For a classical and powerful example, see K. Smith, L. F. Mollenauer, *Opt. Lett.* **14**, 1284 (1989).
7. E. Betzig, J. K. Trautman, T. D. Harris, J. S. Weiner, R. L. Kostelak, *Science* **251**, 1468 (1991).
8. R. C. Reddick, R. J. Warmack, T. L. Ferrel, *Phys. Rev. B* **39**, 767 (1989).
9. M. L. M. Balistreri *et al.*, *Opt. Lett.* **24**, 1829 (1999).
10. J. R. Krenn *et al.*, *Phys. Rev. Lett.* **82**, 2590 (2000).
11. S. I. Bozhevolnyi, J. Erland, K. Leosson, P. M. W. Skovgaard, J. M. Hvam, *Phys. Rev. Lett.* **86**, 3008 (2001).
12. M. L. M. Balistreri, J. P. Korterik, L. Kuipers, N. F. van Hulst, *Phys. Rev. Lett.* **85**, 294 (2000).
13. A. Nesci, R. Dändliker, H. P. Herzig, *Opt. Lett.* **26**, 208 (2001).
14. X. S. Xie, R. C. Dunn, *Science* **265**, 361 (1994).
15. V. Emiliani, T. Günther, C. Lienau, R. Notzel, K. H. Ploog, *Phys. Rev. B* **61**, 10583 (2000).
16. M. Achermann *et al.*, *Appl. Phys. Lett.* **76**, 2695 (2000).
17. J. R. Guest *et al.*, *Science* **293**, 2224 (2001).
18. For a recent review, see J. W. P. Hsu, *Mat. Sci. Eng. Rep.* **R33**, 1 (2001).
19. M. L. M. Balistreri, J. P. Korterik, L. Kuipers, N. F. van Hulst, *J. Lightwave Technol.* **19**, 1169 (2001).
20. Group and phase velocity of the pulse in the channel waveguide are calculated with the effec-
21. The pulse intensities used in the experiment are low enough to prevent nonlinear processes such as self–phase modulation. As a result, the spectral content (and thus the coherence time) of the pulses does not change in either of the branches of the interferometer. Because the measurement is closely related to a field correlate, the length of the pulse as it is found inside the structure is given to first order by the coherence time of the pulse times the velocity at which the pulse travels inside the structure. These considerations lead to an expected pulse length of 71 ± 8 μm.
22. The signal in Fig. 4 is proportional to $I(x,y) = \int dt\, A_{sig}(x,y,t)\, A^*_{ref}(t)\, \cos[\phi(x,y,t)]$. Here A_i denotes the envelopes of the pulses in the signal and reference branches, and $\phi(x,y,t)$ is the phase difference between the two branches. x and y are the coordinates along and perpendicular to the propagation direction, respectively. The reference time has been chosen so that optimal interference is achieved for $x = 0$. It is clear that $I(x,y)$ has a highly similar appearance to the cross-correlation $\Xi(\tau)$. However, because the pulse envelope A_{sig} propagates at a different speed than the phase information, x cannot be translated to a single time delay τ.
23. We thank K.-J. Boller, J. P. Brugger, and D. Lohse for a critical reading of the manuscript. The research described in this report is part of the Strategic Research Orientation of the MESA$^+$ Research Institute on Advanced Photonic Structures. The work was financially supported by the Dutch Foundation for Fundamental Research on Matter (FOM).

Dielectrophoretic Assembly of Electrically Functional Microwires from Nanoparticle Suspensions

Kevin D. Hermanson, Simon O. Lumsdon, Jacob P. Williams, Eric W. Kaler, Orlin D. Velev*†

A new class of microwires can be assembled by dielectrophoresis from suspensions of metallic nanoparticles. The wires are formed in the gaps between planar electrodes and can grow faster than 50 micrometers per second to lengths exceeding 5 millimeters. They have good ohmic conductance and automatically form electrical connections to conductive islands or particles. The thickness and the fractal dimension of the wires can be controlled, and composite wires with a metallic core surrounded by a latex shell can be assembled. The simple assembly process and their high surface-to-volume ratio make these structures promising for wet electronic and bioelectronic circuits.

The assembly of colloidal particles holds promise for the miniaturization of photonic and electrical circuits and their stacking in the third dimension (*1*, *2*). Important recent developments in the field of creating miniaturized electrically functional structures include the synthesis of electronic elements by templated growth in membrane channels (*3*) and their assembly and characterization (*4*, *5*), formation of electrical connections and electronic elements by electrodeposition (*6*, *7*), and assembly of prefabricated blocks by capillary forces (*8*, *9*). Different types of semiconductor nanowires have been synthesized by chemical or electrochemical growth (*10*, *11*) and could be used in prototypes of elec-

Center for Molecular and Engineering Thermodynamics, Department of Chemical Engineering, University of Delaware, Newark, DE 19716, USA.

*To whom correspondence should be addressed. E-mail: odvelev@unity.ncsu.edu
†Present address: Department of Chemical Engineering, Riddick Hall, North Carolina State University, Raleigh, NC 27695, USA.

tronic devices (*12*, *13*). Microwires have also been fabricated by a combination of templating and microfluidics (*14*). In most cases, however, the connection and interfacing of the small elements remains a challenge. Another challenge is to assemble structures from suspension, creating "wet" electronic circuits that can find application in sensors, electrically readable bioarrays, and biological-electronic interfaces.

We report a new class of microwires of micrometer diameter and millimeter length that are assembled from a simple colloidal system of metallic nanoparticles suspended in water. The assembly is based on the mobility and interactions of particles caused by alternating electric fields, commonly referred to as dielectrophoresis (DEP). The alternating current (ac) field allows manipulation and assembly of the particles without the interference of electro-osmotic and electrochemical effects present in direct current (dc) systems. DEP has previously been used as a tool in the fabrication of complex particles (*15–17*), microscopic sensors (*18*), and manipulation of living cells (*19*).

Microwires form after introduction of a suspension of gold nanoparticles of diameter 15 to 30 nm into a thin chamber above planar metallic electrodes deposited on a glass surface (*20*). The gap between the electrodes varies from 2 mm to more than 1 cm, but can also be as small as a few micrometers. When an alternating voltage of 50 to 250 V and frequency of 50 to 200 Hz is applied to the planar electrodes (resulting in a field intensity of ~250 V/cm), thin metallic fibers begin to grow on the electrode edge facing the gap. The fibers grow through the liquid in the direction of the field toward the other electrode at a speed that is typically ≈50 μm/s, but in some cases can be up to an order of magnitude higher so that the gap can be bridged in less than 30 s (see Fig. 1A for typical length scales). When the wire is completely assembled, there is a clear and sharp jump in the electrical current through the cell.

The finding that dielectrophoretic forces can readily assemble nanometer-sized metallic particles from aqueous suspensions into long, electrically conductive microwires is unexpected and is not directly predicted by theory. The dielectrophoretic forces result from the ac field–induced dipoles in the particles and operate in any type of environment and on any type of particle. The first component of these forces is the attractive electrostatic interaction between the dipoles directed along the electric field, similar to that causing particle chaining in electrorheological and magnetorheological fluids (*21–24*). The chaining of millimeter-sized metallic particles, suspended in organic media, has been described and studied previously (*25*, *26*). Our estimates, however, have shown that the

attractive interaction energy between 15- to 30-nm-diameter particles separated by a gap of a few nanometers is negligibly small (*27*). Thus, direct chaining of gold nanoparticles is not theoretically possible and was not seen experimentally.

Microwire growth is caused by particle aggregation at the tip of the fibers, thereby extending them toward the opposite electrode [Movie 1 in the supplementary Web material (*28*)]. The tip of a growing microwire creates local fields of high intensity and gradient, giving rise to a second component of the dielectrophoretic force, which arises from the interaction of the particle dipoles with the nonuniform ac field and is directed along the field gradient (*15–17*, *21*, *22*). For gold particles, this gradient-dependent force leads to the concentration of the particles at the end of the growing tip. Purple coronas of highly concentrated areas in front of the growing wire ends and depletion zones behind them are observed at low nanoparticle concentrations (Fig. 2A). Thus, we believe that microwire formation is a collective effect, whereby the nanoparticles are highly concentrated at the end of the tip and subsequently aggregate to extend the wire in the direction of the field gradient. A broadly analogous effect can be observed in sedimenting colloidal suspensions, in which particles at the bottom pack and aggregate when the effective weight force of the particle column above exceeds the repulsive force between the particles, even though the gravitational force on any single particle is too small to cause coagulation. These gold nanoparticle suspensions are weakly stabilized by electrostatic repulsion and therefore can be made to

coagulate relatively easily. Complex electrohydrodynamic interactions are also likely to be involved in the assembly process because circular flow of the liquid near the end of the growing wires is also commonly observed.

On the basis of these principles, the wire growth process can be controlled in a variety of ways. The wire growth direction is controlled by disturbing the homogeneity of the electric field. This is most easily done by introducing conductive objects in the gap between the electrodes. Such objects create a gradient in the electric field and cause the wire to grow toward them. For example, when small islands of (conductive) carbon paint are deposited in the gap, the wires grow in their direction and spontaneously connect these islands to both electrodes (Fig. 1, B and C). More complex structures involving multiple connections between multiple conductive islands can be formed with time (Fig. 2B).

The effects of the field strength, frequency, particle size and concentration, and electrolyte concentration on microwire growth are summarized in Table 1. The field strength and particle concentration are of major importance, because they must exceed a threshold value in order for the wire to start growing. The effect of the field is anticipated, because the DEP forces depend on the squared values of the field intensity and gradient, and the aggregation can proceed only when the effective force of DEP attraction between the particles and the wire becomes stronger than the electrostatic repulsion of the counterion atmosphere. The threshold effect of the nanoparticle concentration emphasizes the collective nature of the assembly, because
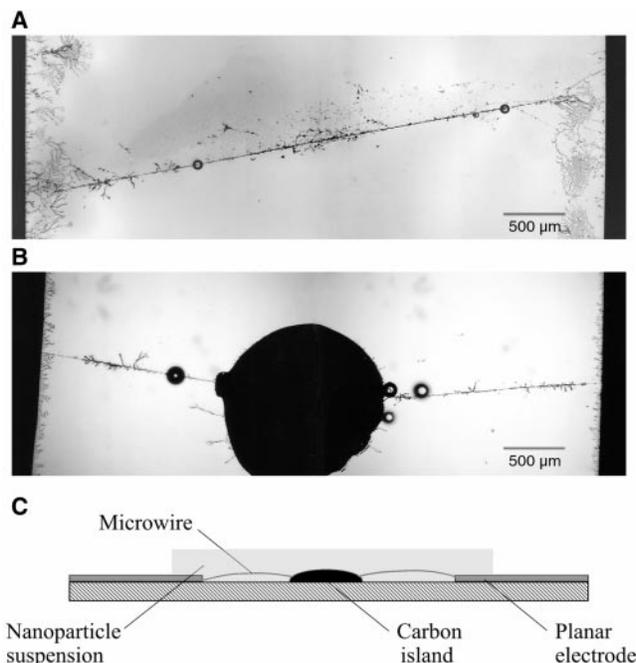

Fig. 1. (**A**) A composite optical micrograph of a gold microwire spanning a 5-mm gap between planar gold electrodes. (**B**) Two wires that have connected to opposite sides of a conductive carbon island deposited in the middle of the gap, and (**C**) schematics of the above configuration.

it implies that aggregation occurs only when the concentration of particles accumulated near the end of the wire is sufficiently high. This finding highlights the importance of dielectrophoretic particle transport to the tips of the microwires, in order to sustain microwire growth and prevent depletion effects at the tips.

The ac frequency should be a less important parameter, although the DEP force is expected to decrease at higher frequencies, which is confirmed by the slowing of wire growth (Table 1). Larger particle sizes should lead to stronger interparticle attractions, more rapid wire growth, and less branching [i.e., a lower fractal dimension (29)]. This is observed experimentally, except for the case of small concentrations of large particles, where depletion effects predominate. Electrolyte concentration should also have a relatively minor effect on the dielectrophoretic attraction, but should enhance particle aggregation by suppressing electrostatic repulsion. These trends are also in accord with the experimental observations, although higher electrolyte concentrations require more electrical power due to the increased current flow through the bulk solution.

The potential usability of these structures in self-assembled circuits depends on their electrical properties in dc and ac modes. The resistivity of the microwires was characterized by two alternative methods. The first was measurement of the current-to-voltage response of single microwires as assembled in the cell. The linear response proves that the wires have a simple ohmic behavior for both ac and dc voltages (Fig. 3A); however, the calculated conductivity is an overestimate because it also includes conductance through the electrolyte between the electrodes.

To measure the true resistivity of the metallic microwire, we added a second pair of electrodes to the cell. This allowed for compensation of the electrolyte conductance (or electrode surface properties) by measurements in a bridge mode [Web fig. 2 (28)]. The length of the microwires was measured from the optical photographs, and the effective diameter from scanning electron micrographs was estimated to be ≈ 1 μm. The specific resistance obtained by these measurements depends on the conditions of assembly and ranges from 3×10^{-6} to 20×10^{-6} ohm·m. This resistivity is about three orders of magnitude higher than that of bulk solid gold and is comparable to that of a number of metallic alloys. This result is perhaps expected because the microwires are assembled from aggregated nanoparticles and their specific conductance will be much lower than that of bulk gold because of their porosity and small interparticle contact areas. The resistances
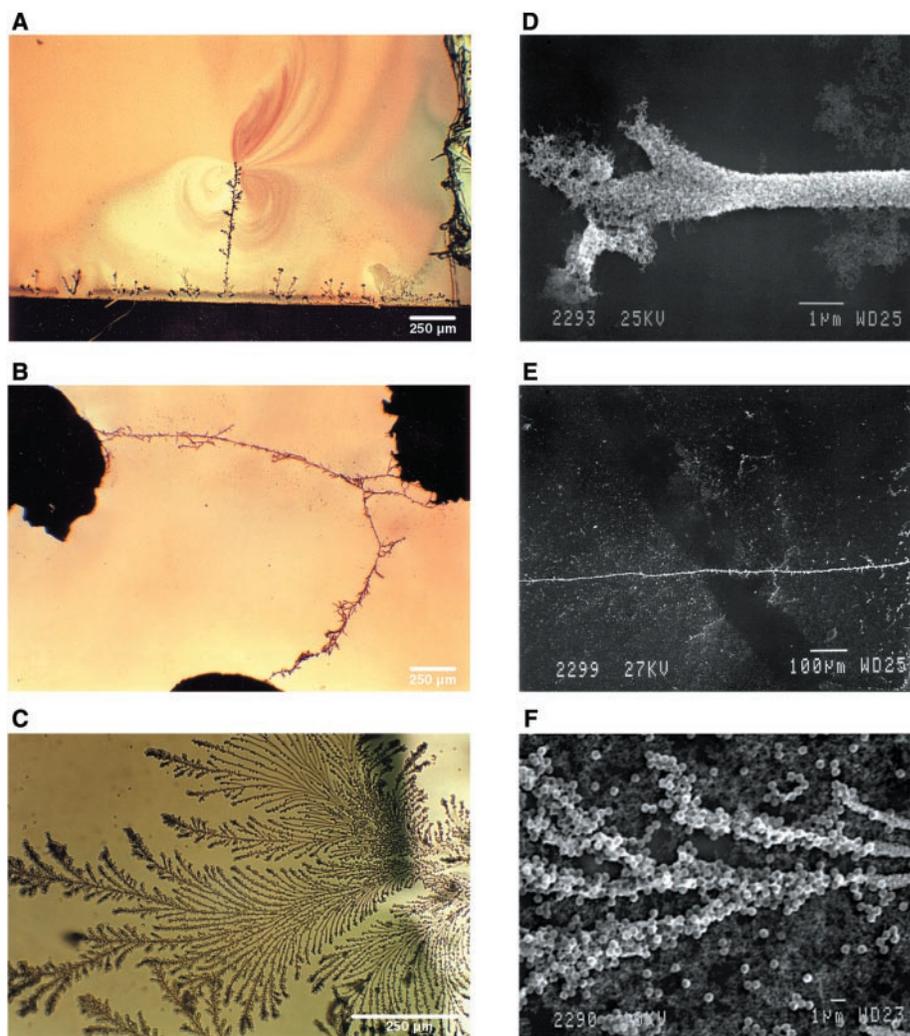

Fig. 2. (**A**) Optical micrograph of a growing wire illustrating the area of high nanoparticle concentration in front of the wire and the depleted area behind. (**B**) More complex connections between three conductive islands. (**C**) Composite wires: a thin fractal gold structure grown on the surface and surrounded by a half-shell of latex microspheres. (**D**) Scanning electron micrograph (SEM) of the end of a growing microwire showing the structure in the growth area and uniform cylindrical porous body. (**E**) SEM of a long, thin microwire. (**F**) SEM of the latex-coated wires (the gold core in the middle is resolved by its higher intensity). Scale bars: (A to C) 250 μm; (D to F) shown on image.
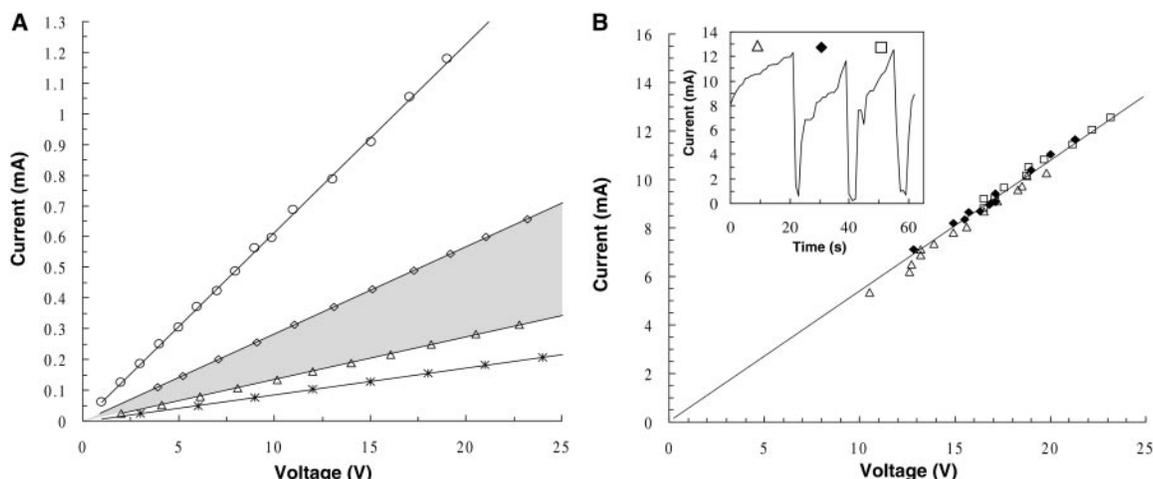
of microwires formed under identical conditions are reproducible (Fig. 3B and the corresponding discussion below). Even though the wires are highly porous, they have good mechanical stability (30).

To explore whether the method can be used to form more complex structures, we grew wires in mixed suspensions of metallic particles and submicrometer-sized polystyrene latex microspheres. As the metallic wire assembly begins, both polymer and gold particles are attracted to and aggregate on the metallic part of the wire tip, thereby forming a metallic structure surrounded by a shell of polymer spheres (Fig. 2, C and F). The specific resistivity of the metallic core was measured to be the same as that of the microwires without the polymer beads assembled from the same suspension and un-

der the same conditions. A variety of core-shell metallo-dielectric structures can potentially be assembled by this method, possibly enlarging the scope of applications of this technology.

A promising aspect of this research is the possibility to quickly and simply create electrical connections at ambient conditions in water environments. Examples of how such wires can connect simple circuits between metallic electrodes and light-emitting diodes are given in Web fig. 3 (28). An interesting and potentially important feature of these self-assembling electrical connections is that they are also self-repairing [Movie 2 in (28)]; that is, if the current through the microwire is increased to the point where the wire breaks and snaps open, the connection is restored by imme-

Fig. 3. (**A**) Examples of the current (*I*) to voltage (*V*) response of a selection of microwires with various lengths and resistivities. The linear dependence demonstrates ohmic behavior with a resistivity in the range of 10^{-5} to 10^{-6} ohm·m. The shaded area outlines the region where the majority (>75%) of responses of the microwires are found. (**B**) Data from an experiment where the microwires are burned out at high voltages, but spontaneously repair to restore the circuit. The inset shows the current response in time. The deep minima following high currents are the intervals of wire disconnection and reassembly. The *I/V* responses of each of the three wires formed in the different cycles are denoted by different symbols. This response is essentially identical for each of the wires and indicates good reproducibility of the properties of microwires assembled under similar conditions.

Table 1. Summary of parameters affecting microwire growth. The general trends are given for three growth characteristics within the ranges studied. The characteristics increase (↑), decrease (↓), or remain constant as each parameter is increased. Additional information on the effect of electrolyte concentration on the appearance and structure of microwires is shown in Web fig. 1 (*28*).

Parameter	Range	Growth rate	Branching	Thickness
Voltage ↑	$23\,\frac{v}{mm} <$ slow $> 40\,\frac{v}{mm}$ fast $> 45\,\frac{v}{mm}$	↑	↓	↓
Frequency ↑	10 Hz < > 150 Hz	↓	↑	↓
Particle concentration ↑	> 0.13%	↑	Constant	↑
Particle size ↑ (constant weight %)	15–30 nm	↓	↓	Constant
Particle size ↑ (constant particle concentration)	15–30 nm	↑	↓	↑
Electrolyte concentration ↑	$(0–3) \times 10^{-4}$ M NaCl	↑	Constant	↑

diate build-up of new nanoparticles in the open gap. This self-repairing is a consequence of the large voltage drop in the small gap between the broken wires. The voltage drop creates a high field intensity, which attracts new particles that aggregate and restore the connection. The data from a cyclic self-repairing process wherein the voltage has been increased to a degree where the wire snaps open and then spontaneously self-repairs to exactly the same resistance are shown in Fig. 3B.

Finally, the microwires can provide chemical sensing functions by virtue of their very high surface-to-volume ratios (*31*). The response of different microwires was monitored after the introduction of a surface functionalization agent, 2-(dimethylamino)ethanethiol hydrochloride, which is known to modify the properties of gold surfaces in solution and to reverse their charge by forming adsorption monolayers (*32*). The wires were formed in the thin flow chamber and their properties were measured in the bridge mode, subtracting the current from the reference electrodes. The initial wire resistivity varied from, e.g., 6×10^{-6} to 20×10^{-6} ohm·m, depending on the electrolyte and nanoparticle concentration as outlined above. In all cases, an easily resolvable and concentration-dependent increase in the resistivity of the microwires was observed after exposure to an analyte. For example, the resistivity increased by ≈10% a few minutes after treatment with 2.5×10^{-4} M thiol solution and ≈7% after treatment with NaCN at pH 11 [Web fig. 4 and Web table 1 (*28*)]. This signal possibly results from a decrease of the surface conductivity of the gold nano-

spheres in the wire structure as they become covered by an organic layer. The signal is probably specific to analytes that modify the counterionic layer around the gold particles. This was validated by an experiment wherein no signal was measured when the solution contained the protein lysozyme, which adsorbs on the gold surface without appreciably affecting its surface conductivity. We believe that such microwire-based chemiresistance sensors can potentially be tailored to specific analytes by surface functionalization with self-assembled monolayers (SAMs). Different SAMs are known to specifically bind ions and small molecules [e.g., (*33*)]. Because the data show that the conductivity response is sensitive to the presence and state of adsorption monolayers, it is likely that it will also be sensitive to the presence of small charged molecules that specifically bind onto the surface of such monolayers.

In conclusion, electrically functional microwires can be formed simply and predictably by the use of dielectrophoresis. The structures reported here cover a new domain in both size and resistivity and close the gap between traditional metallic wires and the more recently synthesized nanowires and carbon nanotubes. Even at this exploratory stage, these wires can perform, for example, as self-repairing electrical leads inside liquid environments and could form the basis of new chemical sensors.

References and Notes
1. G. Decher, M. Eckle, J. Schmitt, B. Struth, *Curr. Opin. Colloid Interface Sci.* **3**, 32 (1998).
2. T. P. Cassagneau, B. Sweryda-Krawiec, J. H. Fendler, *MRS Bull.* **25**, 40 (2000).
3. J. S. Yu *et al.*, *Chem. Commun.* **24**, 2445 (2000).
4. P. A Smith *et al.*, *Appl. Phys. Lett.* **77**, 1399 (2000).
5. J. K. N. Mbindyo *et al.*, *Adv. Mater.* **13**, 249 (2001).
6. J. C. Bradley *et al.*, *Nature* **389**, 268 (1997).

7. J. C. Bradley, Z. M. Ma, S. G. Stephens, *Adv. Mater.* **11**, 374 (1999).
8. N. Bowden, A. Terfort, J. Carbeck, G. M. Whitesides, *Science* **276**, 233 (1997).
9. T. L. Breen, J. Tien, S. R. J. Oliver, T. Hadzic, G. M. Whitesides, *Science* **284**, 948 (1999).
10. J. D. Holmes, K. P. Johnston, R. C. Doty, B. A. Korgel, *Science* **287**, 1471 (2000).
11. T. Thurn-Albrecht *et al.*, *Science* **290**, 2126 (2000).
12. Y. Huang, X. F. Duan, Q. Q. Wei, C. M. Lieber, *Science* **291**, 630 (2001).
13. Y. Cui, Q. Q. Wei, H. K. Park, C. M. Lieber, *Science* **293**, 1289 (2001).
14. P. J. A. Kenis, R. F. Ismagilov, G. M. Whitesides, *Science* **285**, 83 (1999).
15. R. Pethig, Y. Huang, X. B. Wang, J. P. H. Burt, *J. Phys. D Appl. Phys.* **25**, 881 (1992).
16. G. Fuhr *et al.*, *Naturwissenschaften* **81**, 528 (1994).
17. T. Müller *et al.*, *J. Phys. D Appl. Phys.* **29**, 340 (1996).
18. O. D. Velev, E. W. Kaler, *Langmuir* **15**, 3693 (1999).
19. R. Pethig, *Crit. Rev. Biotechnol.* **16**, 331 (1996).
20. The gold suspensions were prepared (*34*) at an Au concentration of 0.01 weight %. The mean size of the particles was determined by dynamic light scattering. The gold suspension was washed three times and concentrated to ~1.5 weight % by centrifugation through a 5000 molecular weight membrane.
21. T. B. Jones, *Electromechanics of Particles* (Cambridge Univ. Press, Cambridge, 1995).
22. H. A. Pohl, *Dielectrophoresis* (Cambridge Univ. Press, Cambridge, 1978).
23. A. P. Gast, C. F. Zukoski, *Adv. Colloid Interface Sci.* **30**, 153 (1989).
24. M. Trau, S. Sankaran, D. A. Saville, I. A. Aksay, *Nature* **374**, 437 (1995).
25. M. Dueweke, U. Dierker, A. Hübler, *Phys. Rev. E* **54**, 496 (1996).
26. W. J. Wen, K. Q. Lu, *Phys. Rev. E* **55**, R2100 (1997).
27. The energy of interaction between two closely situated polarizable particles can be approximated by $w_{max} = -C\pi\varepsilon R^6 K^2 E^2/r^3$, where R is the particle radius, r the distance between the centers, E the intensity of the field, and ε the dielectric permittivity of the media. The Clausius-Mossotti function, K, for metallic particles is ≈ 1 and the factor C ranges from 8 to more than hundreds, depending on the distance between the particles, the higher-order multipole effects, and the number of particles in a chain (*21*, *22*). Even for values of C above 1000, the estimated interaction energy between nanoparticles is smaller than 10^{-2} kT (kT being the thermal energy).
28. Supplementary Web material is available on *Science* Online at www.sciencemag.org/cgi/content/full/294/5544/1082/DC1.
29. The microwire fractal dimensions ranged from 1.01 to 1.71. The Hausdorff dimensions were calculated by computing the density-density correlation function from digitized pictures of the microwires (*35*), assuming that the narrow chamber restricts the growth to two dimensions. At higher voltages, segment rearrangement during growth yields microwires of lower dimension.
30. Rough estimates of the mechanical properties of the microwires are given by their response to the viscous flow of liquid in the flow cell. The wires remain intact after thousands of load/unload cycles of pulsing liquid flow. In addition, the application of voltage between the electrodes immediately restores snapped wires.
31. Any porous conglomerate of gold particles can be expected to display similar changes in resistivity because of surface functionalization (*36*). However, the microwires provide a number of advantages as compared with, for example, deposited strips of gold particles. The wires have more efficient mass transfer, provide sampling through the bulk of the liquid rather than on a surface, can be made as small as necessary, and are formed and automatically connected by self-assembly, rather than by mask deposition or microprinting.
32. C. D. Bain *et al.*, *J. Am. Chem. Soc.* **111**, 321 (1989).
33. R. R. Shah, N. L. Abbott, *Science* **293**, 1296 (2001).
34. J. W. Slot, H. J. Geuze, *Eur. J. Cell Biol.* **38**, 87 (1985).
35. M. Matsushita, M. Sano, Y. Hayakawa, H. Honjo, Y. Sawada, *Phys. Rev. Lett.* **53**, 286 (1984).
36. C. Z. Li, H. Sha, N. J. Tao, *Phys. Rev. B* **58**, 6775 (1998).
37. This work was supported by the National Science Foundation (grant CTS-9986305). The critical comments and support of A. Lenhoff and R. Lobo are gratefully acknowledged. J.P.W. participated in this work as a summer research student from the Department of Chemical Engineering, Carnegie Mellon University (Pittsburgh, PA), and was supported by the NSF (REU grant EEC-9820322).

Oscillations in Phanerozoic Seawater Chemistry: Evidence from Fluid Inclusions

Tim K. Lowenstein,[1]* Michael N. Timofeeff,[1] Sean T. Brennan,[1] Lawrence A. Hardie,[2] Robert V. Demicco[1]

Systematic changes in the chemistry of evaporated seawater contained in primary fluid inclusions in marine halites indicate that seawater chemistry has fluctuated during the Phanerozoic. The fluctuations are in phase with oscillations in seafloor spreading rates, volcanism, global sea level, and the primary mineralogies of marine limestones and evaporites. The data suggest that seawater had high Mg^{2+}/Ca^{2+} ratios (>2.5) and relatively high Na^+ concentrations during the Late Precambrian [544 to 543 million years ago (Ma)], Permian (258 to 251 Ma), and Tertiary through the present (40 to 0 Ma), when aragonite and $MgSO_4$ salts were the dominant marine precipitates. Conversely, seawater had low Mg^{2+}/Ca^{2+} ratios (<2.3) and relatively low Na^+ concentrations during the Cambrian (540 to 520 Ma), Silurian (440 to 418 Ma), and Cretaceous (124 to 94 Ma), when calcite was the dominant nonskeletal carbonate and K-, Mg-, and Ca-bearing chloride salts, were the only potash evaporites.

The long-held consensus that the major-ion chemistry (Na^+, K^+, Ca^{2+}, Mg^{2+}, Cl^-, SO_4^{2-}, HCO_3^-) of the global ocean has remained close to its present-day composition during the Phanerozoic (*1*) (~540 Ma to the present) is at odds with the record of secular changes in the primary mineralogy of marine limestones and evaporites. During the Phanerozoic, the primary mineralogy of nonskeletal limestones has twice oscillated between calcite and aragonite seas (*2*), while over the same interval of 540 million years (My), late-stage salts in marine evaporites have fluctuated between the KCl and $MgSO_4$ types, in step with the calcite-aragonite oscillations (*3*). Current hypotheses for these 100- to 200-My cycles in limestone and evaporite mineralogies involve secular variation in the major-ion chemistry of seawater produced by changes in mid-ocean ridge hydrothermal brine fluxes driven by oscillations in seafloor spreading rates (*3*), as well as seawater-driven dolomitization (*4*). Here, we evaluate secular changes in seawater chemistry in the Phanerozoic through analysis of fluid inclusions.

Bedded halite from marine evaporites as old as the Late Precambrian contains preserved "chevron" crystals formed by primary precipitation on the floor of an evaporating brine body (*5*). These chevron crystals contain bands of primary fluid inclusions parallel to the crystal growth faces, indicating that the inclusions hold trapped surface brines. Individual fluid inclusions in chevron halite are difficult to analyze by extraction techniques because of their dense packing and small size. This problem was overcome by using a scanning electron microscope (SEM) coupled to an x-ray energy-dispersive system (EDS) to directly analyze the major ions in frozen fluid inclusions as small as 30 μm (*6*). An improved SEM-EDS approach using an environmental SEM (ESEM-EDS) allows direct observation and analysis of the surface of frozen fluid inclusions (*7*). Here, we present new ESEM-EDS analyses of fluid inclusions from Late Precambrian, Cambrian, Silurian, Permian, Cretaceous, and modern halites (*8*). Our data are from chevron halites that appear petrographically to be primary (i.e., unrecrystallized). We supplemented our data with published Permian (*9, 10*) and Tertiary (*11*) fluid inclusion analyses.

Fluid inclusions from halites (Fig. 1) trace out paths on Mg^{2+} and Na^+ versus Cl^- plots that reflect changes in brine composition consistent with progressive evaporative concentration in the halite field. Such brine evolution paths support the textural evidence that the inclusions analyzed were trapped during various stages of evaporation of surface brines and not during burial. None of the ancient fluid inclusions, or the evaporation paths they define,

[1]Department of Geological Sciences and Environmental Studies, State University of New York, Binghamton, NY 13902, USA. [2]Department of Earth and Planetary Sciences, Johns Hopkins University, Baltimore, MD 21218, USA.

*To whom correspondence should be addressed. E-mail: lowenst@binghamton.edu